Effective wave propagation along a rough thin-elastic beam

Sebastian Rupprecht[a], Luke G. Bennetts[b], Malte A. Peter[a,c]

[a]*Institute of Mathematics, University of Augsburg, 86135 Augsburg, Germany*
[b]*School of Mathematical Sciences, University of Adelaide, Adelaide 5005, Australia*
[c]*Augsburg Centre for Innovative Technologies, University of Augsburg, 86135 Augsburg, Germany*

Abstract

Two methods for computing the complex-valued effective wavenumber of a rough beam in the context of linear time-harmonic theory are presented. The roughness of the beam is modelled as a continuous random process of known characteristic length and root-mean-square amplitude for either the beam mass or the beam rigidity. The first method is based on a random sampling method, with the effective wave field calculated as the mean of a large ensemble of wave fields for individual realisations of the roughness. The individual wave fields are calculated using a step approximation, which is validated for a deterministic problem via comparison to results produced by an integral equation approach. The second method assumes a splitting of the length scale of the fluctuations and an observation scale, employing a multiple-scale approximation to derive analytical expressions for the effective attenuation rate and phase change. Numerical comparisons show agreement of the results of the random sampling method and the multiple-scale approximation for a wide range of parameters. It is shown that the effective wavenumbers only differ by a real constant between the cases of varying beam mass and rigidity.

Keywords: Wave attenuation, effective wavenumber, elastic beam in vacuo, step approximation, integral equation, multiple-scale approach

1. Introduction

Wave propagation through rough media has long been a topic of interest, e.g. in acoustics and electromagnetics (see the book by Sheng [1]). The effective wave field, i.e. the mean wave field with respect to an ensemble of individual realisations, is often the quantity of interest. Specifically, the effective wavenumber or its change from the wavenumber of the underlying uniform medium, $\bar{k}$,

---

is sought. Computation of the effective wave field and/or effective wavenumber can be numerically intensive. Alternatively, analytic theories can be employed, but their range of validity has to be carefully investigated. The analytic theories include (i) asymptotic theories, often for long waves compared to the length scale associated with the roughness (homogenisation limit, e.g. Kohn and Vogelius [2] considered effective plate equations for vanishing plate thickness and rapidly varying fluctuations), (ii) perturbations from an underlying periodic setting (as discussed for a one-dimensional acoustics problem in Maurel et al. [3]) and (iii) closure assumptions (e.g. the coherent potential approximation, as in Bennetts and Peter [4]).

Solution methods have predominantly been developed for problems in which the roughness originates from discrete scatterers (inclusions or variations in the medium). For this class of problem, it is common to use analytic theories known as Foldy's method or the quasi-crystalline approximation, as described by Linton and Martin [5] for a two-dimensional acoustics problem. Direct numerical computations, in which the effective wave field is calculated as the mean of a large ensemble of wave fields for randomly generated realisations of the roughness, are typically based on addition theorems, such as Graf's formulae in two-dimensions. Often, they employ the fast multipole method (e.g. Gimbutas and Greengard [6]) or other domain decomposition methods (e.g. Montiel et al. [7]) to accelerate computations for large numbers of scatterers. The numerical methods capture the effective wave field up to an arbitrary degree of accuracy, but rely on, e.g., least-squares fitting to extract the effective wavenumber.

In contrast, we assume the fluctuations to be continuous, and defined by a Gaussian autocorrelation function with a prescribed characteristic length, l_{G}, and root-mean-square (roughness) amplitude, ε. More specifically, we consider the one-dimensional problem of linear wave propagation along an infinitely long thin-elastic beam in vacuo. The underlying differential equation is of fourth order, making the problem considerably more difficult than related problems of second order, e.g. in standard acoustics of membrane problems. The roughness is a long patch of either rapidly fluctuating mass or rigidity. This corresponds to the roughness entering in the coefficients of the differential operator at zeroth or second order, respectively. For a uniform beam the wavenumber is real, but the effective wavenumber for a rough beam is complex, with the imaginary component causing the effective wave field to attenuate over the rough interval. The two quantities of interest are the effective phase change and the effective attenuation rate (constituting the deviation of real part of the effective wavenumber from the wavenumber of the underlying wave forcing and the imaginary part of the effective wavenumber, respectively).

A numerical method and an analytical method are presented. The numerical method is based on a version of the step approximation outlined by Bennetts et al. [8] for a water-wave problem. In this approach, each individual realisation of the continuous rough profile is replaced by discrete steps, permitting the individual wave fields to be calculated via an efficient iterative scheme. As described above, the effective wave field is then computed by averaging a large ensemble of realisations, and the components of the effective wavenumber are

extracted by least-squares fits. We validate the wave field produced by the step approximation for a deterministic problem, by comparing it to the wave field produced using an integral equation approach.

The analytical method is based on a multiple-scale approximation, similar to the approach of Kawahara [9] (again, for a water-wave problem). A separation of scales is assumed, where the local characteristic length is of the order of the wavelength as well as the characteristic length. The observation scale, L_{ob}, over which effective properties are sought, is assumed much larger, $L_{\mathrm{ob}} = l_{\mathrm{G}}/\varepsilon^2$, with $\varepsilon \ll 1$. The dependent quantities are then assumed to have a two-scale expansion in ε and individual problems are found to be satisfied by each term in the expansion. Passage to mean quantities allows us to derive an analytical expression for the complex-valued effective wavenumber.

We show that the multiple-scale approximation and the step-approximation method predict the same phase changes and attenuation rates, as long as ε is small enough (~ 0.1). It turns out that the effective wavenumbers only differ by a real constant between the cases of varying beam mass and rigidity. One consequence of the constant difference is that although the phase change tends to zero in the limit $\bar{k}l_{\mathrm{G}} \to 0$ for varying mass, it tends to a finite constant for the varying rigidity. Moreover, the effective wavelength of the rough medium is found to be longer than that of the underlying incident wave forcing in the case of varying mass but shorter for the case of varying rigidity.

The paper is organised as follows: We introduce the problems with varying mass and varying rigidity in § 2. The step approximation and method to generate rough profiles are described in § 3, followed by validation of the step approximation using an integral equation method (described in Appendix A). The multiple-scale approximation is presented in § 4, first for varying mass and then for varying rigidity. Numerical results are given in § 5, showing agreement of the two approaches and discussing their advantages and disadvantages. Moreover, the relation of the effective wave field and wave fields for individual realisations of the roughness are discussed. A summary and discussion of the results of the paper are given in § 6.

2. Preliminaries

We consider an infinitely long thin beam in vacuo. The problem is one-dimensional in the horizontal coordinate x. The spatial part $u(x)$ of the beam deflection $\mathrm{Re}\{u(x)\mathrm{e}^{-\mathrm{i}\omega t}\}$ satisfies the linear thin-beam equation

$$\partial_x^2\big(b(x)\,\partial_x^2 u(x)\big) - \alpha\,g(x)\,u(x) = 0, \qquad x \in (-\infty, \infty), \tag{2.1}$$

where $\alpha = \omega^2$ is the angular frequency squared, and b and g are the beam rigidity and mass density, respectively. Eqn. (2.1) is derived on the basis that no deformations occur in the plane of the beam cross-section and that during deformation, the cross-section remains plane and normal to the deformed axis of the beam (e.g. Bauchau and Craig [10]). In the following, we consider the problems of (i) a beam with a varying mass $g(x)$ (caused by density variations),

fluctuating about the mean $\bar{g}$, and (ii) a beam with varying rigidity $b(x)$ (due to varying Young's modulus), fluctuating about the mean $\bar{b}$.

The varying mass is defined as $g(x) = \bar{g}(1+\varepsilon\gamma(x))$, with $\varepsilon \ll 1$ and $\gamma = \mathrm{O}(1)$. The fluctuations, $\varepsilon\gamma(x)$, have a known characteristic length, l_{G}, and root-mean-square amplitude, ε, which is referred to as the (non-dimensional) roughness amplitude. These are defined via a Gaussian autocorrelation function, which is introduced in § 3.3. The assumption $\varepsilon \ll 1$ is made for consistency with the multiple-scale method in § 4, although this is not required in general, up to the point at which the variations are large enough to produce intervals of negative mass ($\varepsilon \approx 0.3$) with non-negligible likelihood. We note that the varying mass problem can be expressed as

$$\partial_x^4 u(x) - k^4(x)\, u(x) = 0, \qquad x \in (-\infty, \infty), \tag{2.2}$$

where the wavenumber $k(x) = (\alpha g(x)/b)^{\frac{1}{4}}$.

In addition to the varying mass problem, we look at the varying rigidity problem, for which the beam mass g is set to be constant such that the underlying beam equation (2.1) becomes

$$\partial_x^2\big(b(x)\,\partial_x^2 u(x)\big) - \alpha\, g\, u(x) = 0, \qquad x \in (-\infty, \infty). \tag{2.3}$$

In analogy to the varying mass setting, the varying rigidity is defined as $b(x) = \bar{b}(1 + \varepsilon\beta(x))$, where $\beta = \mathrm{O}(1)$ has the same properties as γ (and $\varepsilon \ll 1$ is assumed for consistency with § 4 again).

3. Step approximation and random sampling

3.1. Step approximation

For the varying mass problem, let the roughness extend over a long, finite interval $x \in (0, L)$ and be constant in the surrounding intervals $(-\infty, 0)$ and (L, ∞). We approximate the varying mass profile by a piece-wise constant function on $M \gg 1$ sub-intervals, with $(-\infty, 0)$ and (L, ∞) the 0th and $(M+1)$th sub-intervals, respectively.

In Fig. 1 we can see an example realisation of a continuous varying mass profile for roughness amplitude $\varepsilon = 10^{-2}$ and non-dimensional correlation length $\bar{k}l_{\mathrm{G}} = 2.5$, and the corresponding step approximation of the profile for which each correlation length is divided into four sub-intervals. (This discretisation method will be used for the numerical results in § 5 and details of profile generation are given in § 3.3.) We denote the value of the wavenumber in the mth sub-interval as k_m, and set it to be equal to the value of the corresponding continuous wavenumber profile at the mid-point. The mean wavenumber $\bar{k} \in \mathrm{O}(1)$ corresponds to the mean mass, i.e. $\bar{k} = (\alpha\bar{g}/b)^{\frac{1}{4}}$.

In the mth sub-interval, the wave field can be expressed as

$$u_m(x) = a_m^{(0)}\, \mathrm{e}^{\mathrm{i}k_m x} + a_m^{(1)}\, \mathrm{e}^{-k_m x} + c_m^{(0)}\, \mathrm{e}^{-\mathrm{i}k_m x} + c_m^{(1)}\, \mathrm{e}^{k_m x}. \tag{3.1}$$
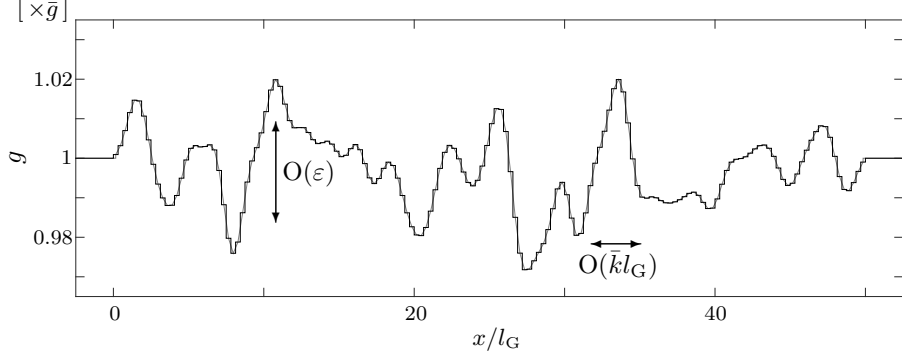
Figure 1: Example realisation of continuous roughness profile (grey curve) and corresponding step approximation with four sub-intervals per correlation length (black) for varying mass problem, for roughness amplitude $\varepsilon = 10^{-2}$ and non-dimensional correlation length $\bar{k}l_G = 2.5$.

The wave amplitudes $a_m^{(0)}$ and $c_m^{(0)}$ correspond to right- and left-travelling waves, respectively, and $a_m^{(1)}$ and $c_m^{(1)}$ correspond to right- and left-decaying evanescent waves. The motion is forced by a unit-amplitude incident wave propagating in the positive x-direction from $x \to -\infty$, which is set via $a_0^{(0)} = 1$ and $a_0^{(1)} = c_{M+1}^{(0)} = c_{M+1}^{(1)} = 0$.

Wave fields in adjacent sub-intervals are coupled via continuity conditions of displacement (u), displacement slope ($\partial_x u$), bending moment ($b\partial_x^2 u$) and shear stress ($\partial_x b\partial_x^2 u$). These continuity conditions are applied at the jumps between the finite sub-intervals within the rough interval, and the jumps at the ends of the rough interval and the surrounding semi-infinite intervals, i.e. at $x = 0, L$. A modified version of the iterative algorithm, presented in Bennetts and Squire [11] for rows of ice floes, is used to calculate the amplitudes $a_m^{(0)}$ and $a_m^{(1)}$ ($m = 1, \ldots, M+1$), and $c_m^{(0)}$ and $c_m^{(1)}$ ($m = 0, \ldots, M$) for a given realisation of the varying mass.

For the problem of varying beam rigidity, the method is applied in an identical fashion but for the step approximation of the rigidity profile, $b(x)$ ($0 < x < L$). For future reference, in this setting we use $\bar{k}$ to denote the wavenumber corresponding to the mean rigidity, $\bar{b}$.

3.2. Validation

The solution given by the step approximation is validated by comparison to the solution given by an integral equation approach outlined in Appendix A. We consider the specific case in which the mass is constant and the rigidity has the single-hump form

$$b(x) = b_0\big(1 + \mu(L/2)^{-8}x^4(x-L)^4\big), \quad x \in (0, L), \tag{3.2}$$

where μ is a prescribed amplitude, and takes the constant value $b(x) \equiv b_0$ in the surrounding semi-infinite intervals. In these semi-infinite intervals, the wave

5

field can be expressed as

$$u(x) = \mathrm{e}^{\mathrm{i}k_0 x} + R^{(0)}\,\mathrm{e}^{-\mathrm{i}k_0 x} + R^{(1)}\,\mathrm{e}^{k_0 x}, \quad x \in (-\infty, 0), \quad\quad (3.3\mathrm{a})$$

$$u(x) = T^{(0)}\,\mathrm{e}^{\mathrm{i}k_0(x-L)} + T^{(1)}\,\mathrm{e}^{-k_0(x-L)}, \quad x \in (L, \infty), \quad\quad (3.3\mathrm{b})$$

where k_0 is the wavenumber corresponding to $b(x) \equiv b_0$, i.e. $k_0 = (\alpha g/b_0)^{\frac{1}{4}}$, and $R^{(0)} \equiv c_0^{(0)}$, $R^{(1)} \equiv c_0^{(1)}$ and $T^{(0)} \equiv a_{M+1}^{(0)}$, $T^{(1)} \equiv a_{M+1}^{(1)}$ are the reflection and transmission coefficients corresponding to travelling (0) and evanescent (1) wave modes.
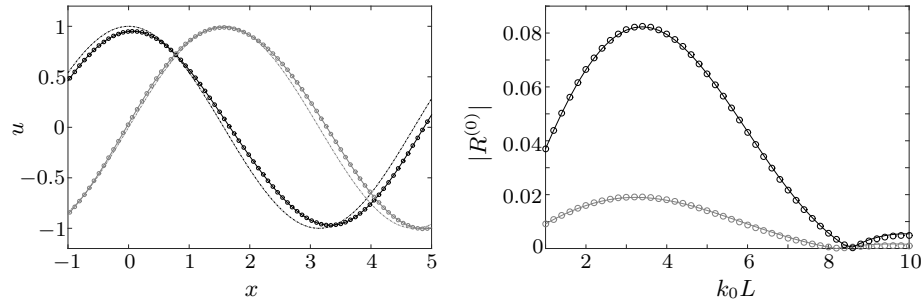

Figure 2: Left-hand panel: Individual wave field for single-hump problem with non-dimensional hump length $k_0 L = 4$ and hump amplitude $\mu = 5 \times 10^{-1}$, computed by integral equation approach (solid line) and step approximation method (∘), split into real part (black) and imaginary part (grey). Components of incident wave are shown for comparison (dash-dotted line with same colour scheme). Right-hand panel: Reflection coefficients for single-hump problem as functions of non-dimensional hump length, for hump amplitudes $\mu = 10^{-1}$ (grey) and 5×10^{-1} (black), computed by integral equation approach (solid line) and step approximation method (∘).

The left-hand panel of Fig. 2 shows real and imaginary parts of the wave field, calculated by the step approximation and integral equation approach for non-dimensional hump length $k_0 L = 4$ and amplitude $\mu = 5 \times 10^{-1}$. For the step approximation, 100 sub-intervals are used over $x \in (0, L)$, in order to obtain a smooth individual wave field, although much coarser resolutions provide sufficiently accurate results in what follows. For the integral equation approach, 4000 sub-intervals are used, which is necessary to capture accurately the reflection of the incident wave for very small hump amplitudes or large hump lengths. It can be observed that the individual wave fields calculated by both methods exhibit very good agreement and that the individual wave fields clearly deviate from the incident wave field, which is also shown for comparison.

The right-hand panel of Fig. 2 shows the absolute values of the (complex-valued) reflection coefficient, $|R^{(0)}|$, as functions of non-dimensional hump lengths, for amplitudes $\mu = 10^{-1}$ and 5×10^{-1}. The two solution methods produce the same reflection coefficients throughout the range of hump lengths considered, $k_0 L \in (1, 10)$. We also observe that the reflection coefficients for $\mu = 10^{-1}$ and 5×10^{-1} share the same qualitative behaviour, attaining maxima at $k_0 L \approx 3.2$ and 3.4, respectively, and zeros at $k_0 L \approx 8.2$ and 8.5, respectively.

3.3. Effective wave field via random sampling

Wave fields are calculated for a large ensemble of randomly generated realisations of roughness profiles, in which profiles share the same amplitude, ε, and characteristic length, l_G. The relationship between an ensemble of beam profiles is expressed via the autocorrelation condition

$$\langle \gamma(x)\,\gamma(x-\xi)\rangle = \rho(|\xi|) \tag{3.4a}$$

for the varying mass problem, and

$$\langle \beta(x)\,\beta(x-\xi)\rangle = \rho(|\xi|) \tag{3.4b}$$

for the varying rigidity problem, where $\langle\cdot\rangle$ denotes the ensemble average of the included quantity with respect to realisations. The autocorrelation is prescribed by the Gaussian autocorrelation function $\rho(|\xi|) = e^{-\xi^2/l_G^2}$ with a characteristic length, l_G, which is referred to as the correlation length from here on.

Following Shinozuka [12], individual realisations of the stochastic processes, $\gamma(x)$ and $\beta(x)$, are generated using a harmonic random process of the form

$$\sqrt{\frac{2}{N}} \sum_{n=1}^{N} \cos\left(r_n x + \varphi_n\right) \tag{3.5}$$

where the frequencies r_n $(n = 1,\ldots,N)$ are random variables independently chosen from a Gaussian distribution with zero mean and standard deviation equal to $\sqrt{2}/l_G$, and the phases φ_n $(n = 1,\ldots,N)$ are independently selected from a uniform distribution over the interval $[0, 2\pi)$. The Wiener–Khinchin theorem and the central-limit theorem can be used to show that expression (3.5) satisfies the Gaussian autocorrelation conditions (3.4a) and (3.4b) in the limit $N \to \infty$. We set $N = 400$ in our random sampling method based on the step approximation, which we refer to in the following for the sake of simplicity as the random sampling method. (With the prescribed approach, the standard deviation of the roughness profiles, with respect to realisations, at all spatial locations x is normalised to unity, and continuity conditions between the rough and semi-infinite intervals are ensured numerically by only considering profile realisations with sufficiently small steps at the respective interfaces.)

The absolute value of the (complex-valued) effective wave field in both problems, $|\langle u\rangle|$, decays exponentially over the rough interval. Hence, the measure of the (real) exponential attenuation rate, Q, is defined via

$$|\langle u\rangle| \propto e^{-Qx}, \qquad x \in (0, L), \tag{3.6a}$$

which is calculated using a least-squares minimisation routine. In addition to the attenuation rate, the (real) phase change, Δk, due to the roughness can be extracted from the ensemble of wave elevations via

$$\langle u\rangle \propto e^{-Qx}\, e^{i(\bar{k}+\Delta k)x}, \qquad x \in (0, L). \tag{3.6b}$$
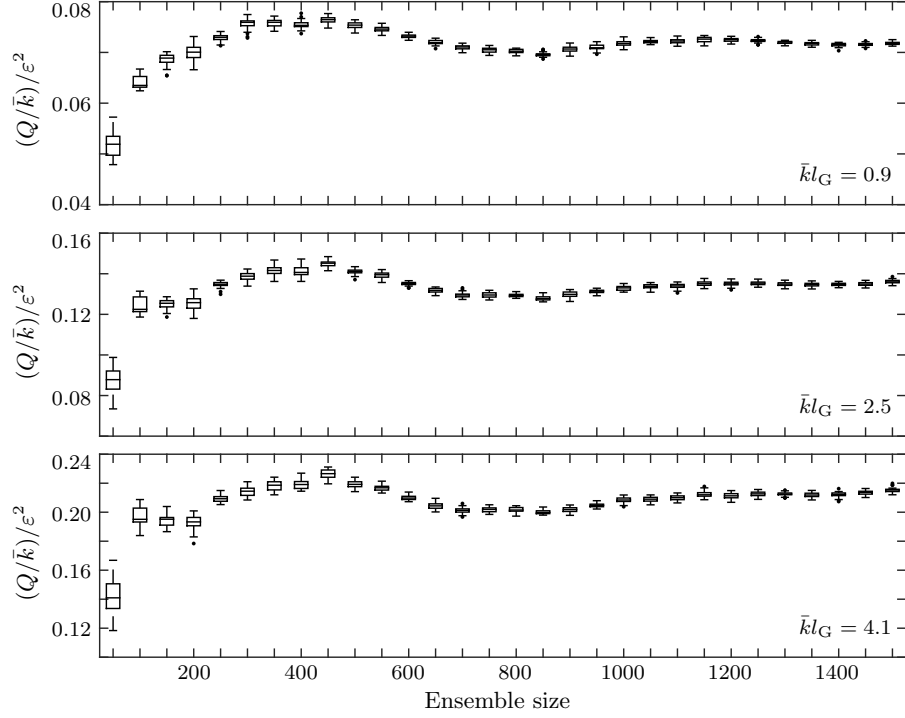
7

Figure 3: Box-and-whisker plots of attenuation rates, as functions of ensemble size (multiples of 50 up to 1500) for varying mass problem, for roughness amplitude $\varepsilon = 5 \times 10^{-2}$ and non-dimensional correlation lengths $\bar{k}l_{\mathrm{G}} = 0.9$ (top), 2.5 (middle) and 4.1 (bottom).

Fig. 3 shows box-and-whisker plots of the effective attenuation rates, as functions of ensemble size (number of profile realisations used in random sampling process), for the varying mass problem with roughness amplitude $\varepsilon = 5 \times 10^{-2}$ and non-dimensional correlation lengths $\bar{k}l_{\mathrm{G}} = 0.9$, 2.5 and 4.1. The attenuation rates are non-dimensionalised with respect to the mean wavenumber, i.e. $Q/\bar{k}$, and scaled by the roughness amplitude squared, ε^2, which proves useful in § 5 where it can be observed that the attenuation rates scale with the square of the roughness amplitude.

For each ensemble size and non-dimensional correlation length, the effective attenuation rates are calculated 40 times to have a sufficiently large sample size for the statistical analysis. The boxes indicate the intervals containing the central 50% of the sampled data (25% to 75% quantiles), and the horizontal lines within them denote the median values (50% quantiles). The whiskers indicate the remaining data lying in the range of 1.5 times the height of the central box next to the quantiles. Points outside this range are considered to be outliers and are shown as bullets.

We can see in Fig. 3 that small ensemble sizes lead to an underprediction of the attenuation of the respective effective wave field for all non-dimensional correlation lengths shown. It takes an ensemble size of approximately 1000

8

to achieve convergence with respect to the attenuation rates. Enlarging the ensemble size beyond 1000 provides greater accuracy, which is indicated by the quantiles moving closer together.

These findings also hold for the phase changes and for the varying rigidity problem (results not shown). In following sections, the ensemble size used to calculate the effective wave fields consist of 1500 randomly generated roughness profile realisations.

4. Multiple-scale approximation

Consider the rough interval to be unbounded, and let the correlation length, l_{G}, represent a local scale and $L_{\mathrm{ob}} = l_{\mathrm{G}}/\varepsilon^2$ an observation scale, for which $\varepsilon \ll 1$ is required. The coordinates x and $x_2 = \varepsilon^2 x$ are used to define locations on the local and observation scales, respectively. We adopt a multiple-scale expansion for the wave field, u, to map the wave field into the new coordinate system, i.e.

$$u(x) = u_0(x, x_2) + \varepsilon u_1(x, x_2) + \varepsilon^2 u_2(x, x_2) + \mathrm{O}(\varepsilon^3). \tag{4.1}$$

By application of the chain rule, the expansion

$$\partial_x u = \sum_j \varepsilon^j \left(\partial_x u_j + \varepsilon^2 \partial_{x_2} u_j \right) \tag{4.2}$$

for the derivative is obtained. The equations to be satisfied by the u_j are derived by substituting the multiple-scale expansion (4.1) into the governing beam Eqn. (2.2) for the varying mass and Eqn. (2.3) for the varying rigidity problem, respectively, and separating the terms with respect to orders of ε.

4.1. Varying mass
4.1.1. Order ε^0

The order ε^0 terms provide the governing equation for the leading-order wave field, u_0, to be

$$(\partial_x^4 - \bar{k}^4) u_0(x, x_2) = 0, \qquad x \in (-\infty, \infty), \tag{4.3}$$

where $\bar{k} = (\alpha \bar{g}/b)^{\frac{1}{4}}$, as defined in § 3.1. Eqn. (4.3) is equivalent to that of a uniform beam. Considering only a right-travelling wave at leading order along the (infinite) rough interval, which is chosen to be consistent with the right incident wave for the finite interval problem in § 3.1, the wave field is

$$u_0(x, x_2) = A(x_2) \, \mathrm{e}^{\mathrm{i}\bar{k}x}, \tag{4.4}$$

where the (complex-valued) amplitude A is now the principle unknown of the problem, and is sought from the higher-order terms. (The intrinsic left-travelling wave is random and can be neglected in this consideration, as can be shown

analogously to the analysis by Bennetts et al. [8].) As the mean wavenumber is fixed with respect to the ensemble, the leading-order effective wave field is

$$\langle u_0(x, x_2)\rangle = \langle A(x_2)\rangle \mathrm{e}^{\mathrm{i}\bar{k}x}, \tag{4.5}$$

with modulus $|\langle u_0(x, x_2)\rangle| = |\langle A(x_2)\rangle|$. It follows that

$$\langle A(x_2)\rangle = A_0\, \mathrm{e}^{\mathrm{i}\Delta k x}\, \mathrm{e}^{-Qx}, \tag{4.6}$$

where A_0 is a constant, and Δk and Q are unknown.

4.1.2. Order ε

Collecting the terms at order ε gives

$$(\partial_x^4 - \bar{k}^4)u_1(x, x_2) = \bar{k}^4\gamma(x)u_0(x, x_2), \quad x \in (-\infty, \infty), \tag{4.7}$$

which is a governing equation for the first-order wave field, u_1, forced by the product of the leading-order wave field, u_0, and the random fluctuation, γ. The solution for a given γ is expressed as

$$u_1(x, x_2) = \bar{k}^4 \int\limits_{-\infty}^{\infty} G(x; \check{x})\gamma(\check{x})u_0(\check{x}, x_2)\, \mathrm{d}\check{x}, \tag{4.8}$$

where G is the Green's function

$$G(x; \check{x}) = \frac{1}{4\bar{k}^3}\left(\mathrm{i}\mathrm{e}^{\mathrm{i}\bar{k}|x-\check{x}|} - \mathrm{e}^{-\bar{k}|x-\check{x}|}\right), \tag{4.9}$$

satisfying the uniform plate Eqn. (4.3), with a unit-amplitude impulse at the source point $\check{x}$, i.e.

$$(\partial_x^4 - \bar{k}^4)G(x; \check{x}) = \delta(x - \check{x}), \quad x \in (-\infty, \infty). \tag{4.10}$$

4.1.3. Order ε^2

The order ε^2 terms give the governing equation for u_2 to be

$$(\partial_x^4 - \bar{k}^4)u_2 = -4\partial_x^3\partial_{x_2}u_0 + \bar{k}^4\gamma(x)u_1, \quad x \in (-\infty, \infty). \tag{4.11}$$

Only the ensemble average of Eqn. (4.11) is required to obtain $\langle A\rangle$, and this is

$$
\begin{aligned}
(\partial_x^4 - \bar{k}^4)\langle u_2\rangle &= -4\langle\partial_x^3\partial_{x_2}u_0\rangle + \bar{k}^4\langle\gamma(x)u_1\rangle \\
&= 4\mathrm{i}k^3\partial_{x_2}\langle A\rangle\mathrm{e}^{\mathrm{i}kx} + 4\bar{k}^3\hat{\zeta}_{\mathrm{vm}}.
\end{aligned}
\tag{4.12}
$$

Here, $\hat{\zeta}_{\mathrm{vm}}$ is the integral

$$\hat{\zeta}_{\mathrm{vm}} = \frac{\bar{k}^5}{4} \int_{-\infty}^{\infty} G(|x - \check{x}|)\langle\gamma(x)\gamma(\check{x})u_0(\check{x}, x_2)\rangle \, \mathrm{d}\check{x}. \tag{4.13}$$

It may be written in the simplified form $\hat{\zeta}_{\mathrm{vm}} = \langle A(x_2)\rangle\zeta_{\mathrm{vm}}$, where ζ_{vm} is a complex constant, defined by

$$\zeta_{\mathrm{vm}} = \frac{\bar{k}^5}{4} \int_{-\infty}^{\infty} G(|\xi|)\mathrm{e}^{\mathrm{i}\bar{k}\xi}\rho(|\xi|) \, \mathrm{d}\xi. \tag{4.14}$$

For the results shown in § 5, the integral in Eqn. (4.14) is calculated numerically using an adaptive quadrature scheme.

Employing the ansatz $\langle u_2\rangle = \mathrm{e}^{\mathrm{i}kx}F(x_2)$, for some function F, the left-hand side of Eqn. (4.12) vanishes, leaving the governing ordinary differential equation

$$\partial_{x_2}\langle A(x_2)\rangle - \mathrm{i}\langle A(x_2)\rangle\,\zeta_{\mathrm{vm}} = 0, \tag{4.15}$$

for the effective amplitude $\langle A(x_2)\rangle$. The solution is

$$\langle A(x_2)\rangle = A_0\,\mathrm{e}^{\mathrm{i}\zeta_{\mathrm{vm}}x_2} \tag{4.16}$$

now, defined earlier giving the phase change, Δk, and attenuation rate, Q, due to the rough mass as, respectively,

$$\Delta k = \varepsilon^2\mathrm{Re}\,(\zeta_{\mathrm{vm}}), \tag{4.17a}$$

$$\text{and} \quad Q = \varepsilon^2\mathrm{Im}\,(\zeta_{\mathrm{vm}}). \tag{4.17b}$$

In particular, this implies that the complex constant ζ_{vm} is the (complex-valued) wavenumber on the observation scale. Moreover, the attenuation rate as well as the phase change predicted by the multiple-scale approximation are proportional to ε^2.

4.2. Varying rigidity
4.2.1. Order ε^0

The governing equation for the leading-order wave field given by the order ε^0 terms for the varying rigidity problem is identical to Eqn. (4.3), where the wavenumber $\bar{k}$ now corresponds to the mean beam rigidity, i.e. $\bar{k} = (\alpha g/\bar{b})^{\frac{1}{4}}$. The solution is again expressed in the form (4.4).

4.2.2. Order ε

The order ε terms give the governing equation for u_1 to be

$$(\partial_x^4 - \bar{k}^4)u_1(x, x_2) = -\partial_x^2\big(\beta(x)\,\partial_x^2 u_0(x, x_2)\big). \tag{4.18}$$

11

As in the varying mass problem, the Green's function (4.9) is used to obtain the solution, with the first-order displacement in this case expressed as

$$u_1(x, x_2) = -\int_{-\infty}^{\infty} G(x; \check{x}) \partial_{\check{x}}^2 \left(\beta(\check{x}) \, \partial_{\check{x}}^2 u_0(\check{x}, x_2) \right) d\check{x}. \tag{4.19}$$

4.2.3. Order ε^2

From the order ε^2 terms, the governing equation for the second-order wave field is

$$(\partial_x^4 - \bar{k}^4) u_2 = -\partial_x^2 \left(\beta(x) \, \partial_x^2 u_1(x, x_2) \right) - 4 \partial_x^3 \partial_{x_2} u_0(x, x_2), \quad x \in (-\infty, \infty), \tag{4.20}$$

with ensemble average

$$\begin{aligned}
(\partial_x^4 - \bar{k}^4)\langle u_2 \rangle &= -4\partial_x^3 \partial_{x_2} \langle u_0(x, x_2) \rangle - \langle \partial_x^2 \left(\beta(x) \, \partial_x^2 u_1(x, x_2) \right) \rangle \\
&= 4\mathrm{i}\bar{k}^3 \partial_{x_2} \langle A \rangle \mathrm{e}^{\mathrm{i}\bar{k}x} + 4\bar{k}^3 \mathrm{e}^{\mathrm{i}\bar{k}x} \langle A(x_2) \rangle \zeta_{\mathrm{vr}},
\end{aligned} \tag{4.21}$$

where ζ_{vr} is the complex constant

$$\zeta_{\mathrm{vr}} = -\frac{1}{4\bar{k}^3} \int_{-\infty}^{\infty} \partial_\xi^2 \left[\partial_\xi^2 G(|\xi|)(\bar{k}^2 \partial_\xi^2 \rho(|\xi|) + 2\mathrm{i}\bar{k}^3 \partial_\xi \rho(|\xi|) - \bar{k}^4 \rho(|\xi|)) \right] \mathrm{e}^{\mathrm{i}\bar{k}\xi} \, d\xi. \tag{4.22}$$

It can be shown analytically by integration by parts and using the field equation for the Green's function, Eqn. (4.9), that

$$\zeta_{\mathrm{vr}} = \zeta_{\mathrm{vm}} + \frac{\bar{k}}{4}. \tag{4.23}$$

As in the varying mass problem, employing the ansatz $\langle u_2 \rangle = \mathrm{e}^{\mathrm{i}\bar{k}x} F(x_2)$ leads us to the ordinary differential Eqn. (4.15), with ζ_{vm} replaced by ζ_{vr}, and solution

$$\langle A(x_2) \rangle = A_0 \mathrm{e}^{\mathrm{i}\zeta_{\mathrm{vr}} x_2}. \tag{4.24}$$

Consequently, the phase change and attenuation rate produced by the varying rigidity are, respectively,

$$\Delta k = \varepsilon^2 \mathrm{Re}\,(\zeta_{\mathrm{vr}}) = \varepsilon^2 \left(\mathrm{Re}\,(\zeta_{\mathrm{vm}}) + \frac{\bar{k}}{4} \right), \tag{4.25a}$$

$$\text{and} \quad Q = \varepsilon^2 \mathrm{Im}\,(\zeta_{\mathrm{vr}}) = \varepsilon^2 \mathrm{Im}\,(\zeta_{\mathrm{vm}}). \tag{4.25b}$$

It is remarkable that the attenuation rates for the varying mass and varying rigidity problem are identical, whereas the phase changes for the two problems agree up to addition of the constant $\bar{k}/4$.
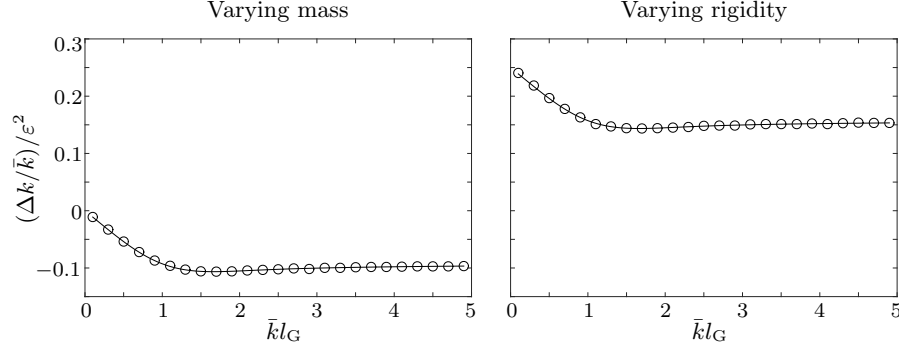
5. Numerical results

Figure 4: Scaled phase changes of the effective wave field as functions of non-dimensional correlation length, for roughness amplitude $\varepsilon = 5 \times 10^{-2}$, predicted by multiple-scale approximation (solid line) and random sampling method ($\circ$) for varying mass problem (left-hand panel) and varying rigidity problem (right-hand panel).

Fig. 4 shows the phase changes. Results are given for the multiple-scale approximation (Eqns. (4.17a) and (4.25a), respectively) and the random sampling method using the interval length $\bar{k}L = 1200$.

For the chosen parameter values, the two methods produce almost identical predictions of the phase changes. For the varying mass problem, the phase change tends to zero as the correlation length tends to zero (the white noise or homogenisation limit). Thus, when the waves are far longer than fluctuations in mass, they only perceive the mean mass. For finite values of the correlation length, the phase change is negative, meaning that the wavelength of the effective wave field is longer than the wavelength corresponding to the uniform beam. The phase change decreases approximately linearly with increasing correlation length over the interval $kl_G \leq 1$, and is approximately constant for $kl_G \geq 1.5$.

In comparison, the offset for the varying rigidity problem is precisely the constant $\bar{k}/4$ from Eqn. (4.23) and the phase change is positive for the varying rigidity problem, meaning that the effective wavelength is shorter than that of the uniform beam. The fact that the phase change is finite as the correlation length tends to zero is presumably because the derivatives of the rigidity appear in the governing Eqn. (2.1).

Fig. 5 shows the corresponding scaled attenuation rates, as functions of non-dimensional correlation length. For these and the following results obtained with the random sampling method, the rough interval length $\bar{k}L = 400 \times \bar{k}l_G$ is used, if not specified otherwise. Again, the agreement between the two methods is nearly perfect, with only small deviations for the smallest correlation length shown, which is caused by numerical difficulties in capturing the very small attenuation rates from the effective wave fields in the random sampling method accurately. The attenuation rates, which are identical for the varying mass and varying rigidity problem produced by the multiple-scale approximation, are
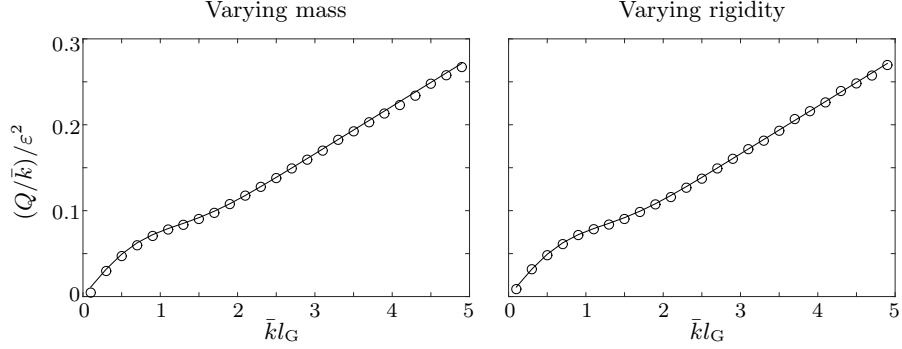
Figure 5: Scaled attenuation rates of the effective wave field as functions of non-dimensional correlation length, for roughness amplitude $\varepsilon = 10^{-2}$, predicted by multiple-scale approximation (solid line) and random sampling method (○) for varying mass problem (left-hand panel) and varying rigidity problem (right-hand panel).

close to zero for the smallest non-dimensional correlation length, $\bar{k}l_{\mathrm{G}} = 0.1$, and increase with increasing correlation length. For $\bar{k}l_{\mathrm{G}} \geq 2$, the attenuation rates are linear with respect to $\bar{k}l_{\mathrm{G}}$.
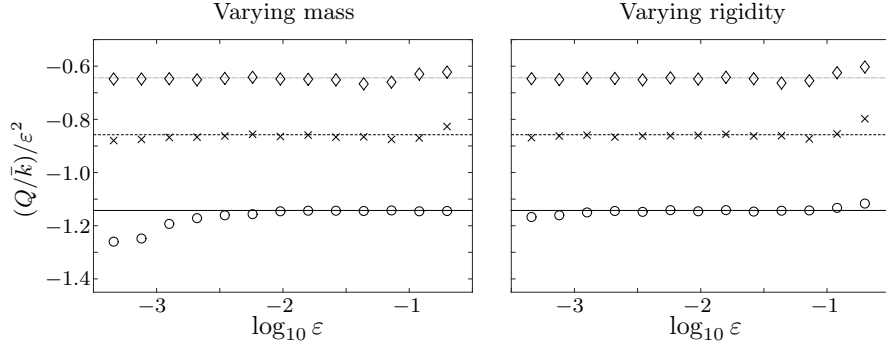
Figure 6: Scaled attenuation rates as functions of roughness amplitude for varying mass problem (left-hand panel) and varying rigidity problem (right-hand panel), predicted by multiple-scale approach (lines) and random sampling method (symbols) for non-dimensional correlation length $\bar{k}l_{\mathrm{G}} = 0.9$ (○, solid line), 2.5 (×, dashed line) and 4.1 (◇, dotted line).

Fig. 6 shows the scaled attenuation rates as functions of roughness amplitude, for the non-dimensional correlation lengths $\bar{k}l_{\mathrm{G}} = 0.9$, 2.5 and 4.1. In general, the multiple-scale approximation and the random sampling method predict the same attenuation rates, confirming that the attenuation rate scales with ε^2 for small ε. Some disagreement is evident for very small values of ε and the smaller values of the correlation length, which, as above, is attributed to numerical difficulties in capturing very small attenuation rates. For $\varepsilon > 0.1$ and particularly for the larger correlation lengths, the attenuation rates predicted by the random sampling method deviate from those predicted by the multi-scale

14

approximation, becoming slightly larger than them. This is a genuine feature and indicates the limit of validity of the multi-scale approximation with respect to ε.
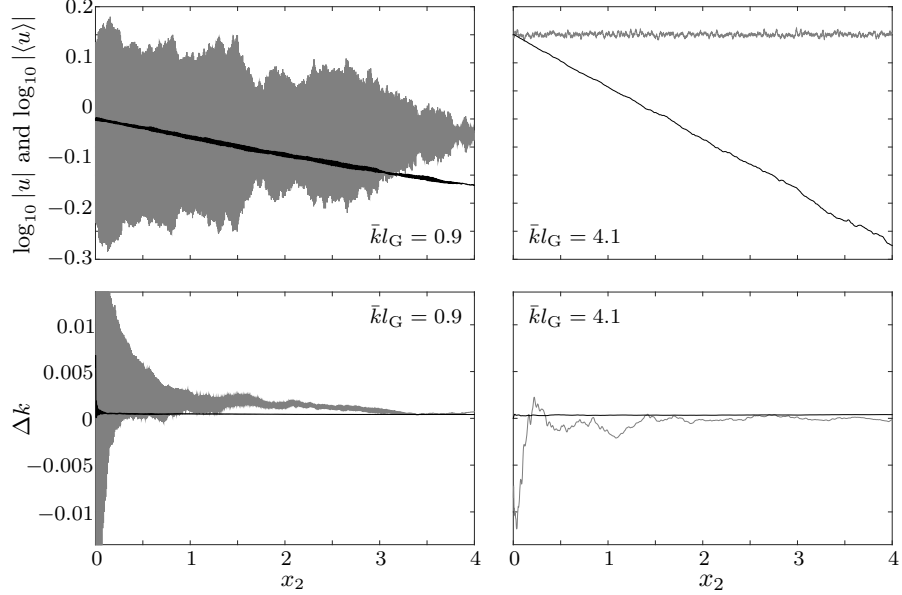

Figure 7: Example individual wave fields (grey curves) and effective wave fields (black) for varying rigidity problem (top panels) and corresponding phases changes (bottom panels, same colour scheme), for roughness amplitude $\varepsilon = 5 \times 10^{-2}$ and non-dimensional correlation lengths $\bar{k}l_{\mathrm{G}} = 0.9$ (left-hand panels) and 4.1 (right-hand panels).

Although this study focusses on the effective wave field, it is informative to compare it to the individual wave fields that form the ensemble — the random sampling method allows us to do this. Fig. 7 shows example individual wave fields and corresponding effective wave fields, for roughness amplitude $\varepsilon = 5 \times 10^{-2}$ and non-dimensional correlation lengths $\bar{k}l_{\mathrm{G}} = 0.9$ (left-hand panels) and 4.1 (right-hand panels). The moduli of the wave fields are shown in the top panels, from which attenuation can be inferred, and phase changes are shown in the bottom panels. The results are for the varying rigidity problem, with corresponding results for the varying mass problem found to be very similar (not shown).

For the attenuation rates, the smaller correlation length, $\bar{k}l_{\mathrm{G}} = 0.9$, is chosen to produce the maximum attenuation of the individual wave fields. Despite this, they attenuate weakly and less than their corresponding effective wave fields. The larger correlation length, $\bar{k}l_{\mathrm{G}} = 4.1$, is chosen to produce strong attenuation of the effective wave fields. In this regime, the fluctuations in the beam are too mild to attenuate the individual wave fields and their moduli randomly fluctuate around unity. It is the de-correlation of the individual wave fields that causes attenuation of the effective wave field. These observations are consistent with

15

those made by Bennetts et al. [8] for water waves propagating over a rough seabed in intermediate water depth, but differ from those of Bennetts and Peter [4], who found similar attenuation rates of individual and effective wave fields for a perturbed periodic array of point scatterers.

The phase changes for the effective wave fields tend (after slight noise for small x) to the values predicted by the multiple-scale approximation shown in Fig. 4. The phase changes for individual wave fields appear to be essentially random.

6. Summary and discussion

We studied effective waves in a rough thin-elastic beam, where the roughness occurs over a long, finite interval, and is in the form of random fluctuations in the beam's mass or rigidity. A step approximation was developed to calculate the beam deflection for a given realisation of the roughness, and the effective wave field was constructed as the mean wave field for an ensemble of randomly generated realisations of the roughness. Phase changes and attenuation rates produced by the roughness were extracted using least-squares minimisation routines. The step approximation was validated for a deterministic problem by comparing it to the solution produced by an integral equation approach, and the convergence of the phase changes and attenuation rates with respect to the size of the ensemble was investigated. Analytic, multiple-scale approximations for the phase changes and attenuation rates were derived, on the assumption that the roughness amplitude is small.

The phase changes and attenuation rates predicted by the random sampling method and the multiple-scale approximation were compared over a range of correlation lengths and roughness amplitudes. The key findings were as follows:

1. The varying mass and varying rigidity produce identical attenuation rates, and identical phase changes up to the addition of a constant.
2. For varying mass, the effective wavelength is longer than the wavelength of the corresponding uniform plate, but it is shorter for the varying rigidity.
3. In the limit that the correlation length tends to zero, the varying mass produces no phase change, but the varying rigidity does produce a phase change.
4. The phase changes and attenuation rates predicted by the random sampling method and the multiple-scale approximation agree up to $\varepsilon \approx 0.1$.
5. The effective wave fields differ from the individual wave fields, particularly in the large-correlation-length regime.

Appendix A. Integral equation solution method

We briefly explain the integral equation approach used in § 3.2. In order to avoid inconveniences originating from the higher-order derivatives, we use a mixed method by introducing the bending moment as an auxiliary unknown and look for the vector-valued function

$$\mathbf{u}(x) = \begin{pmatrix} u(x) \\ b(x)\partial_x^2 u(x) \end{pmatrix}. \tag{A.1}$$

Defining

$$\mathbf{M}(x) = \begin{pmatrix} 0 & 1/b \\ \alpha g & 0 \end{pmatrix} \quad \text{and} \quad \mathbf{M}_0 = \begin{pmatrix} 0 & 1/b_0 \\ \alpha g & 0 \end{pmatrix}, \tag{A.2}$$

the beam equation (2.1) reads

$$\partial_x^2 \mathbf{u} - \mathbf{M}\mathbf{u} = 0 \tag{A.3}$$

in terms of this new unknown. Using an associated matrix-valued Green's function,

$$\mathbf{G}(x;\check{x}) = \begin{pmatrix} \bar{G}(x;\check{x}) & \hat{G}(x;\check{x}) \\ \bar{H}(x;\check{x}) & \hat{H}(x;\check{x}) \end{pmatrix}, \tag{A.4}$$

satisfying

$$\partial_x^2 \mathbf{G}(x;\check{x}) - \mathbf{G}(x;\check{x})\mathbf{M}_0 = \delta(x-\check{x})\mathbf{I} \tag{A.5}$$

as well as the usual radiation conditions where $\mathbf{I}$ is the two-dimensional identity matrix and δ is the delta distribution, Eqn. (A.3) can be converted to the integral equation

$$\mathbf{u}(x) = \mathbf{u}^{\mathrm{I}}(x) + [\partial_x \mathbf{G}(x;\,\cdot\,)\mathbf{u}]_0 - [\partial_x \mathbf{G}(x;\,\cdot\,)\mathbf{u}]_L - [\mathbf{G}(x;\,\cdot\,)\partial_x \mathbf{u}]_0$$

$$+ [\mathbf{G}(x;\,\cdot\,)\partial_x \mathbf{u}]_L + \int_0^L \mathbf{G}(x;\check{x})\left(\mathbf{M}(\check{x}) - \mathbf{M}_0\right)\mathbf{u}(\check{x})\,\mathrm{d}\check{x}, \tag{A.6}$$

where $\mathbf{u}^{\mathrm{I}}(x)$ is the incident wave and $[\,\cdot\,]_x$ denotes the jump of the included quantity at the point x. The components of $\mathbf{G}$ can be found from the standard Green's function for the beam equation with constant coefficients, Eqn. (4.9),

and $\bar{k}$ replaced by k_0, noting that

$$\partial_x^4 \hat{G}(x; \check{x}) - \alpha g b_0^{-1} \hat{G}(x; \check{x}) = b_0^{-1} \delta(x - \check{x}) \tag{A.7a}$$

$$\partial_x^2 \hat{G}(x; \check{x}) = b_0^{-1} \bar{G}(x; \check{x}) \tag{A.7b}$$

$$\partial_x^4 \bar{H}(x; \check{x}) - \alpha g_0 b_0^{-1} \bar{H}(x; \check{x}) = \alpha g \delta(x - \check{x}) \tag{A.7c}$$

$$\partial_x^2 \bar{H}(x; \check{x}) = \alpha g \hat{H}(x; \check{x}) \tag{A.7d}$$

from Eqn. (A.5).

For the numerical approximation of the solution of Eqn. (A.6), we discretise the interval $[0, L]$ by $0 = x_1 < x_2 < \cdots < x_{N-1} < x_N = L$ and use a collocation method, in which we discretise the integral using the compound trapezoidal rule.

The jump terms for the function are treated as essential conditions whereas the jump terms involving the derivatives are kept in the equation as natural conditions. For this purpose, the derivatives are approximated by difference quotients. This leads to the following system of $2N+4$ equations for the $2N+4$ unknowns $\left(\mathbf{u}(x_1), \ldots \mathbf{u}(x_N), R^{(0)}, R^{(1)}, T^{(0)}, T^{(1)}\right)$

$$
\begin{aligned}
\mathbf{u}(x_j) = {} & \begin{pmatrix} e^{ik_0 x_j} \\ b_0 (ik_0)^2 e^{ik_0 x_j} \end{pmatrix} \\
& - \mathbf{G}(x_j; x_1) \left((\mathbf{u}(x_2) - \mathbf{u}(x_1))/h - \left(\begin{pmatrix} ik_0 \\ (ik_0)^3 \end{pmatrix} + \begin{pmatrix} -ik_0 & k_0 \\ (-ik_0)^3 & k_0^3 \end{pmatrix} \begin{pmatrix} R^{(0)} \\ R^{(1)} \end{pmatrix} \right) \right) \\
& + \mathbf{G}(x_j; x_N) \left(\begin{pmatrix} ik_0 & -k_0 \\ (ik_0)^3 & (-k_0)^3 \end{pmatrix} \begin{pmatrix} T^{(0)} \\ T^{(1)} \end{pmatrix} - (\mathbf{u}(x_N) - \mathbf{u}(x_{N-1}))/h \right) \\
& + h \Big(\frac{1}{2} \mathbf{G}(x_j; x_1)(\mathbf{M}(x_1) - \mathbf{M}_0)\mathbf{u}(x_1) + \frac{1}{2} \mathbf{G}(x_j; x_N)(\mathbf{M}(x_N) - \mathbf{M}_0)\mathbf{u}(x_N) \\
& + \sum_{n=2}^{N-1} \mathbf{G}(x_j; x_n)(\mathbf{M}(x_n) - \mathbf{M}_0)\mathbf{u}(x_n) \Big), \quad j = 1, \ldots, N, \tag{A.8a}
\end{aligned}
$$

$$\mathbf{u}(x_1) = \begin{pmatrix} 1 \\ (ik_0)^2 \end{pmatrix} + \begin{pmatrix} 1 & 1 \\ (-ik_0)^2 & k_0^2 \end{pmatrix} \begin{pmatrix} R^{(0)} \\ R^{(1)} \end{pmatrix}, \tag{A.8b}$$

$$\mathbf{u}(x_N) = \begin{pmatrix} 1 & 1 \\ (ik_0)^2 & (-k_0)^2 \end{pmatrix} \begin{pmatrix} T^{(0)} \\ T^{(1)} \end{pmatrix}, \tag{A.8c}$$

where $h = L/(N - 1)$, k_0 is the ambient wavenumber and we have used the continuity of $\mathbf{G}$ at $x = 0, L$. Moreover, we have taken the incident wave to be of unit amplitude, i.e. $e^{ik_0 x}$, and the reflection and transmission coefficients $R^{(0)}, R^{(1)}, T^{(0)}$ and $T^{(1)}$ derive from Eqns. (3.3).

If high accuracy in the reflection and transmission coefficients is required and the problem is such that these are small in value, it may be advisable to enforce all boundary conditions as essential boundary conditions. In this case, the terms in brackets behind the Green's function in the second and the third line of (A.8a) are set to zero as separate conditions. In turn, they drop from

(A.8a), which is then only to be satisfied for $j = 2, \ldots, N-1$.

In general, a Galerkin approach could be used alternatively to solve Eqn. (A.6) or the equivalent integro-differential formulation in terms of u only. In this case, care has to be taken in the choice of test and trial functions owing to the presence of the derivatives.

References

[1] P. Sheng, Introduction to wave scattering, localization and mesoscopic phenomena, Springer, 2006.

[2] R. V. Kohn, M. Vogelius, A new model for thin plates with rapidly varying thickness, Int. J. Solids & Structures 20 (1984) 333–350.

[3] A. Maurel, P. Martin, V. Pagneux, Effective propagation in a one-dimensional perturbed periodic structure: comparison of several approaches, Waves in Random and Complex Media 20 (2010) 634–655.

[4] L. G. Bennetts, M. A. Peter, Spectral analysis of wave propagation through rows of scatterers via random sampling and a coherent potential approximation, SIAM J. Appl. Math. 73 (2013) 1613–1633.

[5] C. M. Linton, P. A. Martin, Multiple scattering by random configurations of circular cylinders: Second-order corrections for the effective wavenumber, J. Acoust. Soc. Am. 117 (2005) 3413–3423.

[6] Z. Gimbutas, L. Greengard, Fast multi-particle scattering : A hybrid solver for the Maxwell equations in microstructured materials, J. Comput. Phys. 232 (2013) 22–32.

[7] F. Montiel, V. A. Squire, L. G. Bennetts, Evolution of directional spectra through finite regular and randomly perturbed arrays of scatterers, SIAM J. Appl. Math. 75 (2015) 630–651.

[8] L. G. Bennetts, M. A. Peter, H. Chung, Absence of localisation in ocean wave interactions with a rough seabed in intermediate water depth, Q. J. Mech. Appl. Math. 68 (2015) 97–113.

[9] T. Kawahara, Effect of random inhomogeneities on nonlinear propagation of water waves, J. Phys. Soc. Japan 41 (1976) 1402–1409.

[10] O. A. Bauchau, J. I. Craig, Structural Analysis - With Applications to Aerospace Structures, volume 163 of *Solid Mechanics and Its Applications*, Springer, 2009.

[11] L. G. Bennetts, V. A. Squire, Wave scattering by multiple rows of circular ice floes, J. Fluid Mech. 639 (2009) 213–238.

[12] M. Shinozuka, Simulation of multivariate and multidimensional random processes, J. Acoust. Soc. Am. 49 (1971) 357–368.